

# Programmable Optical Data Transmission Through Multimode Fibres Enabling Confidentiality by Physical Layer Security

Stefan Rothe<sup>\*,1</sup>, Karl-Ludwig Besser<sup>2</sup>, David Krause<sup>1</sup>, Robert Kuschmierz<sup>1</sup>, Nektarios Koukourakis<sup>1</sup>, Eduard Jorswieck<sup>\*,2</sup>, and Jürgen W. Czarske<sup>\*,1,3</sup>

<sup>1</sup>*TU Dresden, Faculty of Electrical and Computer Engineering, Laboratory of Measurement and Sensor System Technique, 01062 Dresden, Germany*

<sup>2</sup>*TU Braunschweig, Faculty of Electrical Engineering, Information Technology, Physics, Institute for Communications Technology, 38106 Braunschweig, Germany*

<sup>3</sup>*TU Dresden, Faculty of Physics, 01062 Dresden, Germany*

*\*Corresponding authors: stefan.rothe@tu-dresden.de, e.jorswieck@tu-bs.de and juergen.czarske@tu-dresden.de*

## Abstract

Complex light transportation phenomena of multimode fibres can be exploited for information-theoretically secure data transmission. The approach called physical layer security is not crackable by quantum computers as it does not rely on mathematical complexity, but on targeted leveraging of properties that are obscured in the physical channel. For its implementation only knowledge of the channel conditions, i.e. the transmission matrix, is required. This allows wiretap code generation, which determine the appropriate mode combination providing secure data transmission. Once the proper combination is launched at the transmitter-side, the message is delivered to the legitimate receiver and, simultaneously, the full decipherment for an eavesdropper is destroyed. This is demonstrated experimentally at presence of an almighty eavesdropper and the fundamental theory is introduced. We harness effects that have long been considered limiting and have restricted the widespread use of multimode fibres opening new perspectives on information-theoretic security in spatial multiplexing communication systems.

## 1 Introduction

The channel capacities in optical networks can be increased by several orders of magnitude by using space-division multiplexing (SDM) in complement to established methods [1]. Contrary to single-mode fibres (SMFs) on which multiplexing is performed through wavelength or polarisation, spatial degrees of freedom accessible with multi-mode fibre (MMF) or multi-core fibres. These advancements are the result of intense research over the past decade, after Chraplyvy predicted the emerging capacity crunch in 2009 and proposed space as a new essential degree of freedom in communications technology [2]. The requirement for sophisticated SDM solutions is particularly important, as the global exchange of data is increasing exponentially [3] and the number of connected devices in the evolution of Internet-of-Things (IoT) applications in the 5G-era and beyond increases dramatically [4], [5]. This development requires not only higher data rates, but also improved security in terms of confidentiality or privacy with low complexity [6].

However, fibre-based data links are prone to various security risks [7]–[9]. In general, fibre cables, especially SMF cables, are susceptible to evanescent attacks at intentionally inserted bending points [10], [11]. In places with high optical power, for example at outputs of amplifiers, eavesdroppers can remain undetected for a long time. In such cases, it is of utmost importance that messages encoded in tapped signals cannot be reconstructed by unauthorised receivers, which is why additional arrangements need to be made for enabling information security.

Within the past decades, an enormous amount of research has been done in the field of quantum communication [12], [13]. Compared to all alternatives, quantum key distribution (QKD) shows the

strong benefit that the achievable security is underpinned by physical laws. Hence, information-theoretical security can be realized. Although hybrid QKD links consisting of both free-space satellite-to-ground and fiber links with a large number of nodes can already be built in practical environments [14], the achievable key rate is still not fulfilling required benchmarks in the GHz-range. The reason for this are, on the one hand, that severe challenges arise by generating single photons at high rates in defined time intervals, e.g. by quantum dots [15], [16]. On the other hand, each additional component used in a QKD system induces undesired photon losses. In particular, this poses enormous challenges for the integratability into multi-mode SDM networks [17]. The benefit of quantum security is also its disadvantage regarding long-haul transmission system, since the realisation of quantum repeaters requires fundamental paradigm shifts in quantum mechanics [18]. Although QKD systems offer information-theoretic security, it is desirable to consider possible alternatives for information security, especially for SDM networks.

Conventionally, sensitive data is secured at high communication layers either through symmetric key or asymmetric key cryptography. However, a common flaw of symmetric cryptographic approaches is the need for key exchange. This drawback is addressed in asymmetric approaches also known as public-key cryptography, where key exchange is omitted. Nevertheless, they are considered weak compared to quantum computers which in the future could ‘efficiently’ solve prime-factorization problems in polynomial time [19]. In Wyner’s seminal paper [20], it was shown that there exists a class of channel codes, so called wiretap codes, which allow a reliable and confidential communication exploiting actual physical channel properties without a key exchange between two users. This work was related to noisy channels and has opened the research field of physical layer security (PLS). Similarly to QKD, PLS achieves completely secure data transmission, i.e. information-theoretic security. However, specific wiretap codes must be determined for a given channel. The key parameter characterising a PLS system is the secrecy rate  $R_S$ , which is the data rate at which information can be transmitted securely. These are confidentially exchanged between legitimate communication parties, transmitter (*Alice*), legitimate receiver (*Bob*) compared to an eavesdropper (*Eve*).

Light propagation through MMF channels is characterised by complex phenomena, such as modal crosstalk, mode-dependent loss (MDL) or fading. Although these effects appear unpredictable in individual scenarios, they can be measured and controlled. This makes the MMF a suitable candidate for implementing PLS into channels where it is the physical carrier of transmitted information. Once the MMF channel properties are known to Alice by transmission matrix (TM) measurements [21]–[24], she is able to provide a sufficiently high-quality reception at Bob through mode-selective precoding following a carefully chosen wiretap code. Simultaneously, this calibration does not apply to the channel between Alice and Eve due to the mismatch to the channel between Alice and Bob. In contrast to Bob, Eve has to perform channel diagonalisation on her own. Thus, by exploitation of the intrinsic physical properties of the communication channel itself, Alice has the opportunity to escalate the asymmetry between Bob and Eve, making it impossible for Eve to decipher tapped data through channel inversion or any other decoding method.

In this paper, we present the first comprehensive experimental study of confidential data transmission using PLS in a MMF-based communication scheme. The approach introduced is implemented to real MMF to which Eve is physically coupled. In a calibration step using digital holography, the TM of the MMF under test is measured. Afterwards, Alice generates an unitary precoding matrix via singular value decomposition (SVD) applied to the measured TM. Through programmable optics such as a spatial light modulator (SLM), Alice performs optical precoding on the transmitter-side. At the same time, Bob holds the corresponding decoding matrix with which he processes what he receives from Alice. This enables compensation for modal crosstalk between Alice and Bob, and diagonalises the TM. Thus, data can be transmitted via spatial sub-channels, which are referred to as data streams in the following. We show a suitable model tailored to the MMF channel for analysing the measured TMs between both channels Alice to Bob and Alice to Eve. The result is a determination of the achievable secrecy rate  $R_S$  of confidentially exchanged data between Alice and Bob using wiretap codes. This allows us to prove that Alice enhances the signal reception of Bob and degrades the channel to Eve through her precoding. To emphasise the potential of our approach, we show implementations on different fibre lengths illustrating the scalability of the proposed PLS scheme. Contrary to conventional public key algorithms based on prime-factorization, e.g. asymmetric key cryptography, instantaneous physical parameters are exchanged within our approach, which cannot be predicted by a quantum computer [25]. We present how the suggested approach can

contribute to post-quantum cryptography and accordingly resist a cryptanalytic attack by a quantum computer.

## 2 Results

### 2.1 Programmable channel diagonalisation for MMFs through singular value decomposition

Wireless networks are established in various areas of society with sensitive data traffic such as banking or social networking, which is why security in such communication environments is a socially relevant issue. Usually, security is provided by encryption techniques on the upper, logical layers of communication, rather than on the lower, physical layers. However, in novel emerging network architectures, applications are implemented, which require a high level of key management or the scalability of computational effort [26]. Especially in IoT applications, mobile devices of low complexity are becoming increasingly relevant, for example, in the field of healthcare monitoring [27]. For this reason, it is necessary to investigate alternative approaches to classical cryptography, since their deployment requires a comparatively high computational capacity [28]. By exploiting physical properties of multiple-input multiple-output (MIMO) channels, it is possible to relieve, e.g. low-complexity receivers of computationally demanding processes. Following this spirit, PLS has become a hot topic especially in wireless communication in recent years enabling information-theoretic security [29]–[31].

Fortunately, it is possible to take methods extensively studied by the wireless community and implement them in the optical domain of MMF. For example, well known MIMO signal processing techniques are used to distinguish between the modes of the MMF with high performance [32]. However, PLS is not straightforwardly transferable to fibre-optical MIMO channels. The challenge is that fundamental signal transmission specifications change by switching the communication environment. One major difference is the choice of appropriate power constraints. While there is typically an average power constraint in wireless systems [33], instantaneous amplitude constraints need to be applied in MMF [34]. The motivation behind this stems from the optical setup where a laser is employed at the transmitter and a camera at the receiver. First, the laser has a finite power output, and second, the camera is calibrated for a certain maximum power to avoid nonlinear fiber effects. Besides power constraints, the nature of the transmission medium itself is fundamentally different in fibre-based communication. Thus, the comprehensive development of appropriate models for the use of PLS in MMF is necessary. Such a transition was introduced by the group of Peter Winzer, for the first time. Achievable security rates in MMF links in the presence of (multiple) eavesdroppers were explored by mathematical models. The proposed idea is to exploit MDLs, which create an asymmetry between legitimate and illegitimate recipients yielding a crucial signal-to-noise ratio (SNR) advantage on favourable modes [11], [35]–[37]. Winzer’s group has shown experimentally, using an SMF data link, that secrecy can be achieved by information scrambling (polarisation-division multiplexed 16-ary quadrature amplitude modulation), but without using an actual MMF or a physically tapped eavesdropper [38].

However, to experimentally validate confidentiality enabled by PLS in an MMF system (see Fig. 1), the measurement of the existing channel matrices is required. In preliminary work [39], we have shown that an SNR advantage for Bob over Eve based on TM measurements can be achieved. However, for determining  $R_S$ , channel matrices between both channels Alice to Bob and Alice to Eve are necessary, which can be provided by measuring the TM of the MMF under test. Since transverse modes are the basis of the available channel, mode-selectivity on Alice’s side is crucial for measuring the TM with a high precision of which can be ensured by using an SLM [40], [41]. Other mode-multiplex techniques such as a tapered SMF array, i.e. photonic lantern, enable access to only mode-groups, when a graded-index MMF is used [42]. On the receiver-side, interferometric measurement techniques like, e.g. digital off-axis holography, are commonly used for retrieving both amplitude and phase information occupying the TM entries with complex coefficients. After the TM has been measured, proper diagonalisation methods can be applied compensating for modal crosstalk between Alice and Bob. In contrast, Eve has to perform channel inversion, which leads to noise amplification. This phenomenon can be additionally exploited crucially by using wiretap codes.

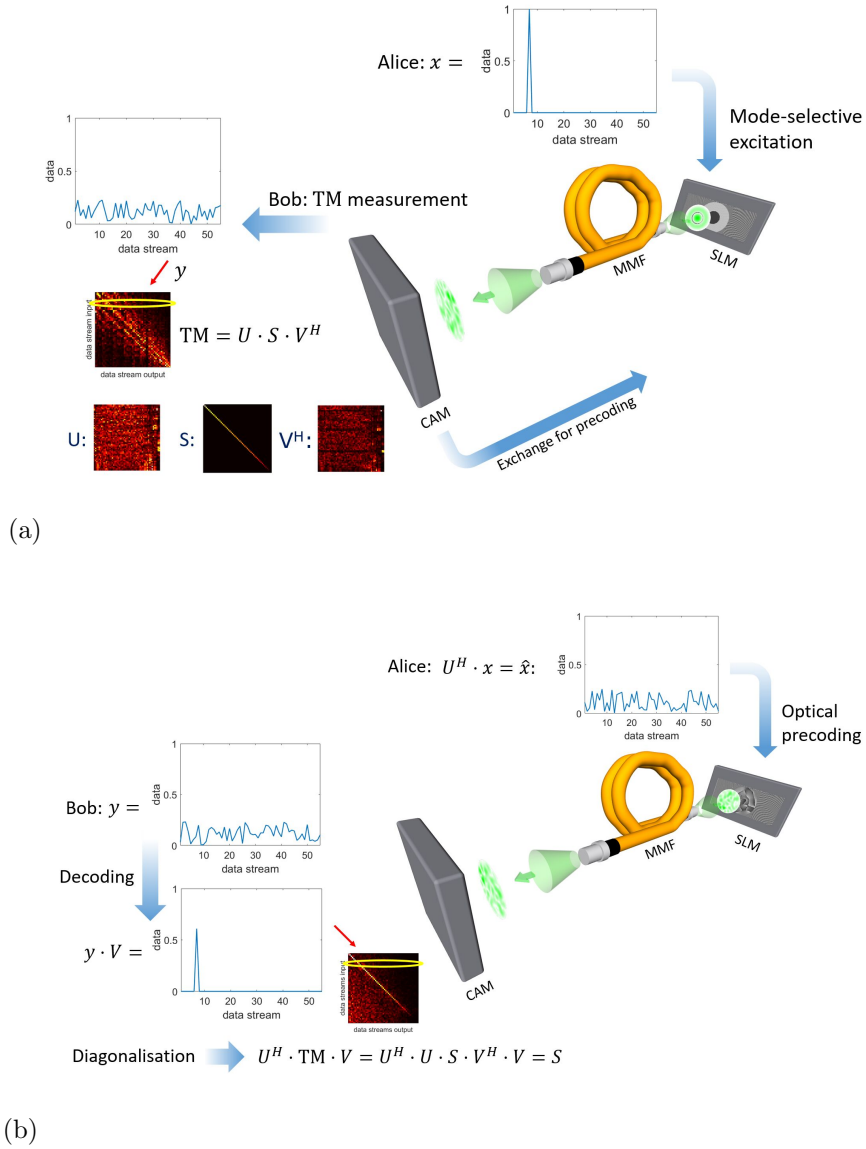


Figure 1: Principle of PLS implemented in an optical MMF scheme. (a) During a calibration phase, Alice and Bob are determining the TM of the MMF under test. Alice uses an SLM enabling mode-selective excitation iterating through each row of the TM. Bob measures the scrambled light field on the receiver-side, holographically. Through mode decomposition, Bob identifies the complex entries of the TM. By using SVD, Alice and Bob are generating both pre- and decoding matrices  $U^H$  and  $V$ , respectively. Amplitude values are shown. (b) By proper SVD pre- and decoding, the MMF channel is diagonalised. Alice applies matrix  $U^H$  for transmission using the SLM, while Bob applies  $V$  for reception equalising their channel. Consequently, spatial data streams are generated which are represented by the diagonal matrix  $S$  in which the channel's singular values are located. Thus, both the number and quality of potential data streams are already available after measuring TM. Matrix  $S$  represents the theoretical optimum of the equalisation, which is why  $S$  provides a benchmark for the experimental implementation of PLS. In the example shown, data transmission is made on data stream 8. The maximum achievable level of the detected signal on this data stream is determined by its singular value, which is  $\sigma_8 = 0.6$  in this particular case.

In wireless communications, channel diagonalisation through SVD is well-established for multi-antenna systems [43], [44]. This includes the area of PLS, where it can be the optimal strategy [45]. For optical

fibre-based MIMO, this method was considered by Ho *et al.* [46] in 2013. However, its feasibility has, to the best of our knowledge, never been shown experimentally, yet. Although TM diagonalisation schemes have been employed for equalization of modal crosstalk in MMFs [23], it has not yet been shown to generate and prove confidential data exchange through MMF MIMO-SDM channels. The hurdle is the correct measurement of the TM with increasing MMF length. During the entire TM measurement, phase-correct measurements on the observing position are crucial for viable light control through the MMF. Usually, the TM is measured in a specific plane on Bob’s side, which is determined by the position of his camera sensor. In this case, phase-correct implies that in each iteration, the phase is measured relative to the absolute reference point, i.e. Bob’s camera. The challenge is, that phase drifts between object and reference paths occur which are induced by environmental influences such as mechanical stress and temperature fluctuations, especially when the reference is provided by a separate SMF. Therefore, the absolute position of the reference point tends to fluctuate between each measurement, i.e. between each line of the TM. This is why a reference measurement monitoring the drift of the camera position is usually involved within TM measurements [47]. In communication applications, increased fibre lengths are desired, due to which phase fluctuations increase in frequency. Thus, phase monitoring becomes more challenging as the frame rates of available SLMs and cameras are limited. This poses an obstacle for TM measurements with long MMFs. In contrast, guide star techniques are considerably more robust against phase drifts. With digital optical phase conjugation [48], the correct phase position between two playbacks is not relevant and setups of up to 1 km long MMF links are straightforwardly implementable [49].

There has already been research to compensate for the drift between object and reference paths at MMF TM measurements. Reference-less approaches bypass the provision of a reference and do not suffer from phase drifts [50]. The stability gained is at the cost of computationally intensive optimisation algorithms that currently require a lot of time. In other work [51], phase stability is increased compared to external reference approaches, when object and reference share a common path through the MMF. Both object and reference experience the same aberrations during propagation and cancel each other when both paths interfere at the MMF output, i.e. receiver facet. In [51], it is claimed that the approach does not suffer from fundamental limitations in fibre length. However, the reference is speckled. Thus, it is not possible to measure the entire complex profile at the receiver facet, which results in so-called ‘blind spots’. Here, we present a development of this approach. We also exploit the phase stability of common-path systems, but ensure a uniform illumination profile of the reference beam in an off-axis configuration. This is achieved by adaptive filtering using a digital micromirror device (DMD). The setup introduced works as a self-referencing plug’n’play solution for holographic TM measurements for long MMF links. Detailed information is provided in the supplementary material. We show measurements on 55-mode MMF with step-index profile at up to 100 m length. Using the TM, pre- and decoding can be realised for channel diagonalisation between the legitimised communication parties generating spatial data streams. Each data stream identifiable from the TM is represented by its singular value. Applying SVD to the measured TM provides:  $\text{TM} = U \cdot S \cdot V^H$ . Alice obtains her precoding matrix  $U^H$ , whereas Bob obtains his decoding matrix  $V$ . These matrices are unitary, which allows both participants to simply multiply them on the transmitter-, or the receiver-side:  $U^H \cdot \text{TM} \cdot V = U^H \cdot U \cdot S \cdot V^H \cdot V = S$ . The remaining matrix  $S$  is a diagonal matrix which has the singular values of TM on its diagonal in descending order. This principle only applies for the channel for which the TM was measured. Therefore, there is a mismatch with the TM to Eve. The proposed principle of PLS in MMF networks is shown in Fig. 1. After Alice multiplies  $U^H$  to her message  $x$ , she receives the mode combination that should be launched using the SLM. The mode combination appears arbitrary (see Fig. 1b), but it is well-defined and matches the decoding procedure on Bob’s side. The mode combination finally excited varies according to the occupation of TM. The performance of this method depends on how well MMF channels can be diagonalised, a characterisation of which is shown in the supplement.

## 2.2 Demonstration of Confidential Data Links

In order to show that a positive secrecy rate  $R_S$  can be achieved for MMF channels, we consider the following transmission scheme. Alice uses binary phase-shift keying (BPSK) at the input, which automatically fulfills the peak-power constraint. With the SVD-based precoding discussed in Section 2.1, we diagonalise the channel to Bob. This allows to transmit  $K$  data streams in parallel by using the subset

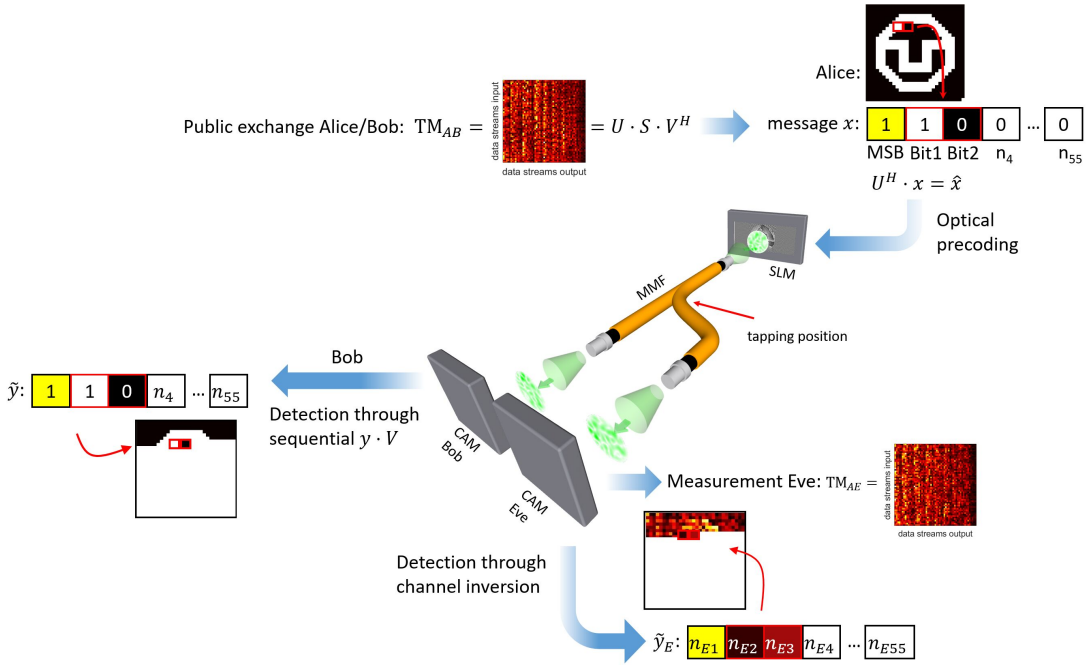
of the  $n$  available spatial degrees of freedom determined by the number of modes the MMF supports. The choice of data streams corresponds to the  $K$  highest singular values. Since the precoding is matched to Bob's channel only, Eve needs to perform a channel inversion to diagonalise her channel. However, this induces a noise amplification for her. A detailed description of the model and transmission strategy can be found in the supplement.

Demonstrating such a transmission through MMF in an experimental environment, we base the analysis of the achievable secrecy on TM measurements. For the specification of  $R_S$  determining how many bits can be transmitted with information-theoretic security, it is required to measure the TM between Alice and Bob as well as between Alice and Eve, cf. Section 4 in the supplementary material. In Fig. 2, the setup for measuring TMs under Eve's presence is shown. In the case of data transmission through the MMF, Eve can physically gain access to the legitimate channel by tapping to it. Usually, Alice and Bob could expose Eve's tapping as the received intensity level on Bob's side would fluctuate, dramatically. However, to evaluate the worst-case scenario from a communication perspective, the TMs for both channels (Alice to Bob,  $TM_{AB}$  and Alice to Eve,  $TM_{AE}$ ) are measured using the same reception conditions for both Bob and Eve including SNR or ambient influences, e.g. mechanical stress or temperature. Therefore, we took 10 m long MMFs and realised Eve's access via 50:50 coupling. In order to account for variations due to different coupling positions, two separate MMFs were used with one coupling 1 m away from Alice and one with 1 m away from Bob, respectively.

For demonstration purposes, an image of the TU Dresden logo was vectorised into a bit sequence and transmitted via the three most favourable data streams corresponding to the three largest singular values after diagonalisation of  $TM_{AB}$ . Note, that in a different case, a different number of data streams could be used in parallel. Within our investigations, the image (see Fig. 2b) has been transmitted without using wiretap codes, at first. In this case, Bob can observe the transmitted image as  $\tilde{y} = y \cdot V$  (see Fig. 2c), which is close to the transmitted one. The striped background in Fig. 2c is due to the repeated transmission sequence of data streams 1, 2 and 3. Data stream 1 serves as most significant bit, while data streams 2 and 3 carry actual data. However, these data streams correspond to different singular values that result in different levels of the respective detected signals. Similarly, Eve can observe her received image as  $\tilde{y}_E$  (see Fig. 2d), which is already a much distorted version of the original image due to noise amplification arising from channel inversion. This effect could be further amplified by transmitting artificial noise [52], for example, or by physical effects such as MDL due to increased mode number or fibre length. However, it can be seen that some information, e.g., the outer shape of the logo, is preserved. Therefore, the transmission is not fully information-theoretic secure and only relies on the mismatch between the SVD precoding and Eve's channel. In order to avoid any information leakage, wiretap codes can be employed [31]. Wiretap codes are a special class of channel codes, which are designed to allow a data transmission that is simultaneously reliable to a legitimate receiver and secure against an eavesdropper. In this work, we apply polar wiretap codes [53] to demonstrate that secure transmissions over wiretapped MMF channels are possible. In a simulation, we digitally implemented them to the measured channels from Fig. 2. These coding methods used are standardised in 5G networks [54] and form the basis for an implementation of the aforementioned calculations along with Monte Carlo (MC) simulations, which can be found at a public repository which we provide [55]. An application to our measurement data produces the results for Bob and Eve shown in Fig. 2e and f, respectively. As can be observed, Bob receives an almost error-free reconstruction of the original image, while Eve receives noise.

The goal for a secure communication network is to have  $R_S$  as large as possible. With the considered BPSK transmission, one can transmit at most one bit per symbol, i.e., the rate for one of the data streams can be 1 at most. Since we assume to use  $K$  out of  $n$  data streams in parallel exploiting the MMF's spatial degrees of freedom, the maximum achievable secrecy rate with this scheme is  $K$  bit per channel use. A detailed analysis of the achievable secrecy rates for this scheme is presented in the supplementary material.

For the measured TMs, we obtain the results presented in Fig. 3. The blue curve shows the secrecy rate for the measured MMF channels where the SVD precoding at Alice is performed within a simulation, i.e., a perfect implementation and therefore an upper bound on the performance. However, for a real data transmission over the fibre, we need to implement the SVD precoding optically with a SLM as shown in Figs. 1 and 2. The secrecy rates for the measured channels with optical precoding are indicated by the yellow curve in Fig. 3. These results are obtained by MC simulations with  $10^5$  samples [55]. For comparison, we show the achievable secrecy rate when no precoding is performed at Alice as the third



(a)

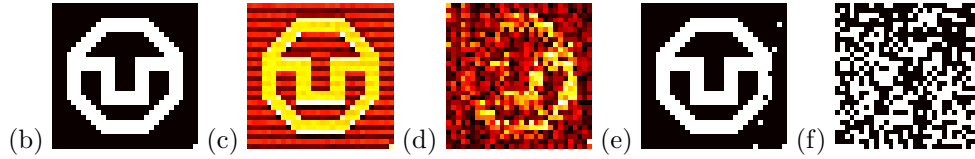


Figure 2: Experimental scheme for quantifying the achievable secrecy rate  $R_S$  in a real data transmission through MMF. After diagonalisation, the logo of TU Dresden is vectorised and transmitted sequentially over the most favourable three data streams represented by the three highest singular values. The first bit serves as most significant bit (MSB). While Alice and Bob perform pre- and decoding based on  $TM_{AB}$  to retrieve the received message  $\hat{y}$ , Eve measures her own TM,  $TM_{AE}$  and performs channel inversion. Afterwards, Eve receives the tapped message  $\tilde{y}_E$ . If the principle of PLS was successful,  $\hat{y}$  contains elements of the transmitted message  $x$ , while at the same time  $\tilde{y}_E$  contains noise. In (b), the original image is shown. (c) and (d) show raw data of the received messages on Bob's and on Eve's side, respectively. These images result from an experimental environment in which Eve's get physical access to 50% of the total power. As explained in Fig. 1, the singular values have different levels in descending order. Therefore, signals on data stream 3 will have a lower level than those on data stream 2. The striped pattern in (c) occurs due to the repeated transmission sequence of data streams 2 and 3. An upgraded toolbox is provided by PLS methods that further degrades the reception conditions on Eve's side while improving those on Bob's side. Using wiretap codes, the vectorised image is translated into an extended code word before transmission. The received messages are evaluated using a decoding matrix that matches the code word. This creates binary sequences for both Bob (e) and Eve (f). The images shown in (e) and (f) were created in a simulation to demonstrate the power of wiretap codes on our raw measured data shown in (c) and (d).

curve in Fig. 3. In this case, the  $K$  data streams are transmitted simply over the first  $K$  modes of the MMF and both receivers employ channel inversion upon reception.

First, it can be seen that a positive secrecy rate is indeed achievable with the considered transmission scheme. The secrecy rate for SVD precoding within a simulation increases with the number of data

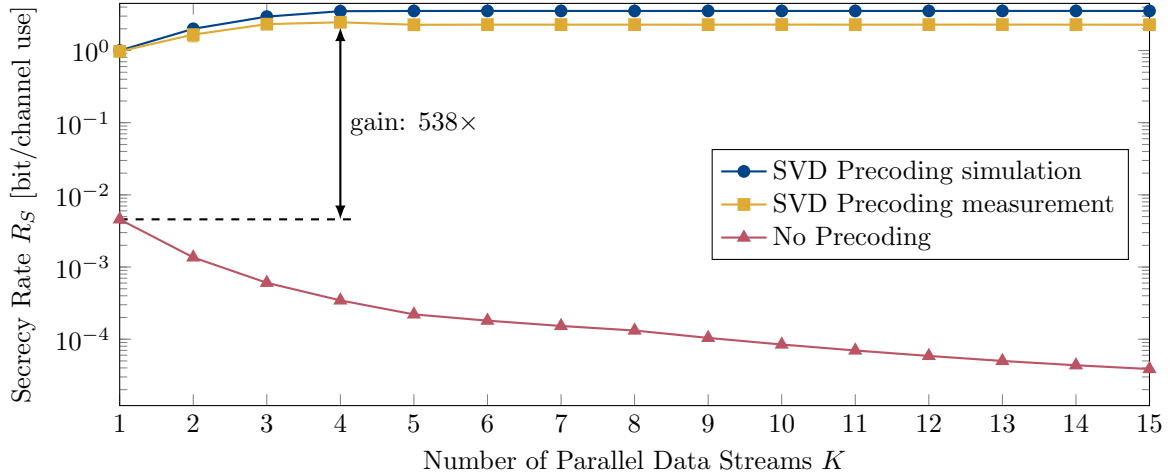


Figure 3: Achievable secrecy rate  $R_S$  of the MMF channels for the described BPSK transmission scheme over the number of used data streams  $K$ . The constant signal power constraint is set to 10 dB. The first curve gives a theoretical upper bound, if the SVD precoding could be implemented perfectly. The second curve is derived from the measurements with actual optical precoding. The third curve provides a comparison to the scenario without any precoding at the transmitter. The lines show the average obtained for multiple measurements of two fabricated MMFs. The indicated gap is computed between the maximum of the second curve and the maximum of the third curve.

streams that are used for data transmission until it saturates. Thus, there is a minimum number of data streams on which data should be sent in parallel achieving the highest possible secrecy rate  $R_S$ . A parallel transmission on more data streams has no further advantage. The reason behind this is that the power for the individual data streams is allocated corresponding to the singular values of  $\text{TM}_{\text{AB}}$ . At high  $K$ , data streams with very small singular values are added and their assigned power is also close to zero. Therefore, the contribution to the secrecy rate is negligible. On the other hand, we find that there is an optimum  $K$  for the actual implemented system that uses a SLM for precoding. In Fig. 1b as well as in Fig. S1a of the supplementary material, it can be seen that the diagonalised channel between Alice and Bob is not a ‘perfect’ diagonal matrix. Recall that this should in theory be a diagonal matrix containing the singular values of  $\text{TM}_{\text{AB}}$  on the main diagonal, as shown in Fig 1a. However, in the practical system, the diagonalisation worked properly for only a few data streams. In Fig. S1b in the supplementary material, it is shown that within the first 10 data streams we achieve a SNR of up to 26 dB. This result corresponds to the channel estimations of other SDM systems that operate with a single MMF core over 45 transverse modes [56]. Even though some of the performance is lost due to the experimental implementation in a real system, the secrecy rate derived from the practical system is close to the upper bound.

In contrast, there is a significant gap from the SVD precoding systems to the scenario where no precoding is used at the transmitter. Recall, that data is transmitted directly on the first  $K$  modes for this particular scenario. In this case, it can be noted that the secrecy rate decreases with an increasing number of data streams. This is due to MDL to the coupled eavesdropper, as the fundamental mode is the one with the least degeneracy and thus less likely to couple. Therefore, when only using this mode for data transmission, Eve gets the least information and the highest secrecy rate is achieved. When adding more modes for data transmission, the power needs to be distributed over the modes and more information is leaked to the eavesdropper.

### 3 Discussion

The use of PLS in MMF communication systems enables to create confidential data connections employing classic light. As PLS exploits complex phenomena of MMFs, it can be applied in high-capacity SDM networks of the future and is based on infrastructure as of today. This opens a new perspective of the



already existing opportunities for information-theoretic secure exchange of sensitive data in fibre optic communication. Our results showcase, that PLS is a serious alternative to other approaches providing information security.

While information-theoretic security is confirmed by physical laws in quantum systems and therefore exists intrinsically, channel codes must be determined for PLS systems. However, one main advantage of PLS is that it achieves post-quantum security because the information leaked to the wiretapper does not allow to obtain the transmitted message, neither with classical nor with quantum computational resources [57]. Similar to QKD systems, PLS achieves information-theoretic and thereby post-quantum security.

In this work, we show an experimental study of PLS on MMF data links, for the first time. Worst-case scenarios were assumed, where legitimate and non-legitimate receivers have identical reception conditions. This means that Bob and Eve each share 50% of the transmitted power. In a practical implementation, an attacker would be revealed at lower power leakage levels since the power drain would be detected by the legitimate receiver. Nevertheless, as results show, the channel between Alice and Bob can be calibrated and data can be transmitted confidentially through 3 parallel spatial data streams. We examined two different coupling positions. One is close to Alice and one is close to Bob. We observed no significant differences under varying coupling positions. We attribute this to the pronounced modal crosstalk occurring in step-index fibres, which is fully developed after short distances. Sometimes, *man-in-the-middle* attacks, where an attacker has access to the entire channel power, are mentioned in literature. However, they are not feasible for fibre-optical data links. Such an attack, unlike in wireless communication networks, would require a disconnection of the link and thus be immediately revealed.

The achievable secrecy rate of PLS strongly depends on fibre parameters and the experimental apparatus for TM measurement, i.e. channel diagonalisation performance. We use simple step-index fibres for our experiments. Compared to gradient index fibres (GRIN), step-index fibres are considered less robust regarding light transport [58]. Thus, light control through them appears to be much more challenging. Therefore, we expect our results to be improved by using GRIN. In our investigations, a parameter configuration was used which allows propagation of 55 modes per polarisation state. The optimal number of modes for PLS incorporates a trade-off between metrological effort and information security benefits. In principle, an increasing number of modes requires a more elaborate measurement of the TM, which is why the lowest possible number of modes is advantageous as each additional mode requires at least one more measurement. In addition, it becomes more challenging to measure the TM for all modes, as more degrees of freedom are required for wavefront shaping. However, with an increasing number of modes, another TM basis such as Hadamard [21] or focal points [22] can be used reducing the experimental effort. On the other hand, an increasing number of modes is advantageous for information security. The more spatial data streams, or sub-channels exist, the more data streams with high singular values to Bob could possibly be used. At long fibre lengths, fluctuations occur which must be considered for interferometric TM measurements. Usually, an SMF provides the required reference, externally. However, if an external reference is used, phase fluctuations between object and reference increases in frequency the longer the distance is. This effect can be reduced by, for example, a much more robust apparatus such as a common-path setup. Therefore, we built an adaptive spectral amplitude filter with which we show diagonalisations for up to 100 m step-index fibre. By upgrading the TM measurement in the PLS system to a common-path configuration, it can be expected that there are no fundamental obstacles with regard to the achievable fibre length [51]. If desired, a more suitable wavelength can be used for long-haul transmission and the link can be extended with a repeater or amplifier. Another required feature of the setup is a high degree of flexibility in wavefront shaping. By diagonalising the channel, the appropriate mode combination needs to be launched as precise as possible on the transmitter-side, which can be realised best by an SLM at the moment. On the receiver-side, a sufficiently high SNR is required for interferometric measurements. Basically, the required SNR is given by the quantum efficiency of the camera sensor, which is mainly influenced by the noise level of possible amplifiers or repeaters between network nodes.

For measuring the whole TM of a 55-mode MMF in one polarisation state, 110 measurements are necessary, where 55 are required for retrieving the rows of the TM, and 55 for reference enabling phase monitoring. Currently, the acquisition takes  $\approx 35$  s, as the SLM can operate at 5 Hz. However, since there is no trigger connection between camera sensors and SLM, there is high potential to further increase the

system’s temporal efficiency. Even though the use of DMDs is extremely lossy, they achieve operation rates that are orders of magnitude higher than those of LCoS displays [21]. Particularly promising are piston-like DMDs whose losses are drastically reduced compared to conventional tip/tilt devices.

Other work has demonstrated comparable data transmission techniques through MMFs using time reversal [49]. The combination of classical light calibration with the transmission of single photons for QKD systems was described. We believe that a calibration technique based on TMs, can also be combined with single photon transmission. In our understanding, channel diagonalisation using TM measurement enables, for example, the SMF-like transmission of single photons through arbitrary mode channels, which allows the implementation of QKD protocols such as BB84 in MMF [59]. Measuring the entire TM provides high information density compared to single playbacks, which is why we assume an increased transmission fidelity by measuring the TM, compared to time reversal.

## 4 Methodology

### 4.1 Transmission Matrix Measurement

Based on preliminary work [60], we measured all TMs in the base of the transverse modes the MMF supports. This choice provides the smallest possible TM dimension. The mode base can be derived by solving Maxwell’s equations [61] depending on the manufacturer’s specifications of both MMF and laser. On Alice’s side, linear polarized LP modes are excited sequentially using an SLM. We use computer generated holograms (CGHs) for complex light field generation to ensure precise launching [62]. In our case, since enough SLM pixels are available, we use superpixels. We believe that other CGH algorithms could produce similar results. Due to modal crosstalk, speckle patterns are received on Bob’s, respectively Eve’s side and imaged onto a camera. The images interfere with a reference wave in an off-axis configuration. Compared to other holographic retrieval techniques using, for example, correlation filters [63], one line of the TM can be measured single-shot. After storage, these holograms are analysed using the angular spectrum method [64] with which amplitude and phase are retrieved. After reconstruction from both complex field components, a mode decomposition is performed to determine modal weights. The result corresponds to one row of the TM. Drifts between object and reference are monitored by a reference measurement. In our case, the fundamental mode is launched after each TM measurement step. We track the evolution of the phase in the fundamental mode, which corresponds to the global phase drift of the system. Phase values between the reference points are interpolated to correct the TM rows for the phase drift [47]. In total, we perform both 55 measurements for the TM as well as for reference. The detailed setup is shown and described in supplementary material.

### 4.2 Fabrication of tapped multimode fibres

Coupling for providing Eve’s access to Alice and Bob’s channel was realised by fibre fusion coupling (ETEK FCPW-2000 Fiber Coupler Production Workstation). We achieved a 50:50 coupling rate using a broadband LED source. We varied tapping positions while maintaining the same coupling conditions. In terms of reproducibility, couplings were carried out on identical 10 m MMF (FG025LJA, step-index,  $\text{\O}25\ \mu\text{m}$ , NA 0.1) links. From the respective tapping position, the distance to Eve’s fibre facet was kept at 1.2 m.

### 4.3 Wiretap Codes

In order to achieve information-theoretic security, wiretap codes can be used as channel codes when transmitting data. Typically, they have a binning structure, where the secret messages of length  $k$  are mapped together with confusion messages of length  $r$  to codewords of length  $n$  [31]. Throughout this work, we assume binary messages and codewords. Thus, for each secret message  $m \in \mathbb{F}_2^k$ , there exist  $2^r$  different codewords  $\mathcal{C}_m \subset \mathbb{F}_2^n$ , i.e., there exists an encoding function  $\gamma_m : \mathbb{F}_2^r \rightarrow \mathcal{C}_m$  that assigns a different codeword to  $m$  depending on the confusion message. The confusion messages are chosen randomly at the transmitter and we therefore have an overall stochastic encoder  $\gamma : \mathbb{F}_2^k \times \mathbb{F}_2^r \rightarrow \mathbb{F}_2^n$  for the wiretap code.

Multiple schemes to construct wiretap codes exist, e.g., based on polar codes [53], low density parity check (LDPC) codes [65], [66], or lattice codes [67].

## 4.4 Evaluation of the achievable secrecy rate with Monte Carlo simulations

The theoretical performance in terms of the achievable secrecy rate can be calculated analytically as shown in Section 4 in the supplementary material. However, this is not easily possible for the measured MMF channels with optical precoding due to the experimental implementation. Instead of exact calculations, we resort to MC simulations to determine the secrecy rate. Based on a large number of randomly generated symbols, we estimate the bit-flip probabilities of the channels to Bob and Eve and use these values for calculating the secrecy rate. The exact implementation to verify all of the presented results can be found at [55].

### Data availability

All presented calculations and MC simulations to verify the analytical results are openly published at [55]. In order to allow reproducing all of the results in this work, we also publish the measured TMs from which the presented results are derived.

### Acknowledgements

The authors thank Jens Peupelmann (IJP, Halsbrücke) for fabricating the tapped fibres. The authors thank Andrew Lonnstrom for fruitful discussion. J. C. and E. J. acknowledge the German Research Foundation (grant no. (CZ 55/42-1) and (JO 801/25-1)) for funding.

### Author contributions

S.R. conducted the optical experiments with assistance from N.K., R.K. and D.K.; K.B. set up the model and carried out secrecy analyses. S.R. and K.B. evaluated the data. J.C., N.K. and E.J. conceived the idea. E.J. and J.C. supervised the work and did project management. All authors contributed to the preparation of the paper.

### Competing interests

The authors declare no competing interests.

### Additional information

#### Supplementary information

**Correspondence** Correspondence to Stefan Rothe (stefan.rothe@tu-dresden.de), Eduard Jorswieck (e.jorswieck@tu-bs.de) and Jürgen W. Czarske (juergen.czarske@tu-dresden.de)

## References

- [1] B. J. Puttnam, G. Rademacher and R. S. Luís, ‘Space-division multiplexing for optical fiber communications,’ *Optica*, vol. 8, no. 9, pp. 1186–1203, 2021.
- [2] A. Chraplyvy, ‘The coming capacity crunch,’ in *35th Eur. Conf. Opt. Commun.*, Vienna, Austria, 2009.
- [3] Cisco. (Mar. 2020). ‘Cisco annual internet report (2018–2023) white paper,’ [Online]. Available: <https://www.cisco.com/c/en/us/solutions/collateral/executive-perspectives/annual-internet-report/white-paper-c11-741490.html> (visited on 26/03/2021).
- [4] M. A. Arfaoui, M. D. Soltani, I. Tavakkolnia, A. Ghayeb, M. Safari, C. Assi and H. Haas, ‘Physical layer security for visible light communication systems: A survey,’ *IEEE Communications Surveys & Tutorials*, 2020.
- [5] M. R. Palattella, M. Dohler, A. Grieco, G. Rizzo, J. Torsner, T. Engel and L. Ladid, ‘Internet of things in the 5G era: Enablers, architecture, and business models,’ *IEEE Journal on Selected Areas in Communications*, vol. 34, no. 3, pp. 510–527, 2016.

- [6] M. P. Fok, Z. Wang, Y. Deng and P. R. Prucnal, ‘Optical layer security in fiber-optic networks,’ *IEEE Transactions on Information Forensics and Security*, vol. 6, no. 3, pp. 725–736, 2011.
- [7] M. Medard, D. Marquis, R. A. Barry and S. G. Finn, ‘Security issues in all-optical networks,’ *IEEE Network*, vol. 11, no. 3, pp. 42–48, 1997.
- [8] K. Shaneman and S. Gray, ‘Optical network security: Technical analysis of fiber tapping mechanisms and methods for detection & prevention,’ in *IEEE MILCOM 2004. Military Communications Conference, 2004.*, IEEE, vol. 2, 2004, pp. 711–716.
- [9] M. Z. Iqbal, H. Fathallah and N. Belhadj, ‘Optical fiber tapping: Methods and precautions,’ in *8th International Conference on High-capacity Optical Networks and Emerging Technologies*, IEEE, 2011, pp. 164–168.
- [10] M.-Y. Loke and J. N. McMullin, ‘Simulation and measurement of radiation loss at multimode fiber macrobends,’ *Journal of lightwave technology*, vol. 8, no. 8, pp. 1250–1256, 1990.
- [11] K. Guan, J. Cho and P. J. Winzer, ‘Physical layer security in fiber-optic MIMO-SDM systems: An overview,’ *Optics Communications*, vol. 408, no. June, pp. 31–41, Feb. 2018. DOI: 10.1016/j.optcom.2017.07.078.
- [12] C. Bennet, ‘Quantum cryptography,’ in *Proc. IEEE Int. Conf. Computers, Systems, and Signal Processing, Bangalore, India, 1984*, 1984, pp. 175–179.
- [13] P. D. Townsend, ‘Quantum cryptography on multiuser optical fibre networks,’ *Nature*, vol. 385, no. 6611, pp. 47–49, 1997.
- [14] Y.-A. Chen, Q. Zhang, T.-Y. Chen, W.-Q. Cai, S.-K. Liao, J. Zhang, K. Chen, J. Yin, J.-G. Ren, Z. Chen *et al.*, ‘An integrated space-to-ground quantum communication network over 4,600 kilometres,’ *Nature*, vol. 589, no. 7841, pp. 214–219, 2021.
- [15] P. Michler, A. Kiraz, C. Becher, W. Schoenfeld, P. Petroff, L. Zhang, E. Hu and A. Imamoglu, ‘A quantum dot single-photon turnstile device,’ *science*, vol. 290, no. 5500, pp. 2282–2285, 2000.
- [16] C. Hopfmann, N. L. Sharma, W. Nie, R. Keil, F. Ding and O. G. Schmidt, ‘Heralded preparation of spin qubits in droplet-etched gas quantum dots using quasis resonant excitation,’ *Physical Review B*, vol. 104, no. 7, p. 075301, 2021.
- [17] N. H. Valencia, S. Goel, W. McCutcheon, H. Defienne and M. Malik, ‘Unscrambling entanglement through a complex medium,’ *Nature Physics*, vol. 16, no. 11, pp. 1112–1116, 2020.
- [18] W. K. Wootters and W. H. Zurek, ‘A single quantum cannot be cloned,’ *Nature*, vol. 299, no. 5886, pp. 802–803, 1982.
- [19] K. Li, P.-G. Yan and Q.-Y. Cai, ‘Quantum computing and the security of public key cryptography,’ *Fundamental Research*, vol. 1, no. 1, pp. 85–87, 2021.
- [20] A. D. Wyner, ‘The wire-tap channel,’ *Bell system technical journal*, vol. 54, no. 8, pp. 1355–1387, 1975.
- [21] O. Tzang, E. Niv, S. Singh, S. Labouesse, G. Myatt and R. Piestun, ‘Wavefront shaping in complex media with a 350 kHz modulator via a 1D-to-2D transform,’ *Nature Photonics*, vol. 13, no. 11, pp. 788–793, 2019.
- [22] M. Plöschner, T. Tyc and T. Čížmár, ‘Seeing through chaos in multimode fibres,’ *Nature Photonics*, vol. 9, no. 8, pp. 529–535, 2015.
- [23] J. Carpenter, B. J. Eggleton and J. Schröder, ‘Complete spatiotemporal characterization and optical transfer matrix inversion of a 420 mode fiber,’ *Optics Letters*, vol. 41, no. 23, pp. 5580–5583, 2016.
- [24] M. Mounaix and J. Carpenter, ‘Control of the temporal and polarization response of a multimode fiber,’ *Nature Communications*, vol. 10, no. 1, pp. 1–8, 2019.
- [25] C. Gidney and M. Ekerå, ‘How to factor 2048 bit RSA integers in 8 hours using 20 million noisy qubits,’ *Quantum*, vol. 5, p. 433, Apr. 2021. DOI: 10.22331/q-2021-04-15-433. arXiv: 1905.09749 [quant-ph].

- [26] H. V. Poor and R. F. Schaefer, ‘Wireless physical layer security,’ *Proceedings of the National Academy of Sciences*, vol. 114, no. 1, pp. 19–26, 2017.
- [27] R. Sharma, A. R. Nair *et al.*, ‘IoT-based secure healthcare monitoring system,’ in *2019 IEEE International Conference on Electrical, Computer and Communication Technologies (ICECCT)*, IEEE, 2019, pp. 1–6.
- [28] A. K. Alharam and W. El-madany, ‘Complexity of cyber security architecture for iot healthcare industry: A comparative study,’ in *2017 5th International Conference on Future Internet of Things and Cloud Workshops (FiCloudW)*, IEEE, 2017, pp. 246–250.
- [29] W. Trappe, ‘The challenges facing physical layer security,’ *IEEE Communications Magazine*, vol. 53, no. 6, pp. 16–20, 2015.
- [30] R. Liu and W. Trappe, Eds., *Securing Wireless Communications at the Physical Layer*. Springer, 2010. DOI: 10.1007/978-1-4419-1385-2.
- [31] M. Bloch and J. Barros, *Physical-Layer Security*. Cambridge University Press, 2011. DOI: 10.1017/CB09780511977985.
- [32] S. O. Arik, J. M. Kahn and K.-P. Ho, ‘MIMO signal processing for mode-division multiplexing: An overview of channel models and signal processing architectures,’ *IEEE Signal Processing Magazine*, vol. 31, no. 2, pp. 25–34, 2014.
- [33] A. Goldsmith, *Wireless communications*. Cambridge University Press, 2005.
- [34] A. W. Snyder and J. D. Love, ‘Optical waveguide theory,’ *Journal of the Optical Society of America A*, vol. 3, no. 3, pp. 378–379, 1986.
- [35] K. Guan, E. C. Song, E. Soljanin, P. J. Winzer and A. M. Tulino, ‘Physical layer security in space-division multiplexed fiber optic communications,’ in *2012 Conference Record of the Forty Sixth Asilomar Conference on Signals, Systems and Computers (ASILOMAR)*, IEEE, 2012, pp. 654–658.
- [36] K. Guan, P. J. Winzer, A. M. Tulino and E. Soljanin, ‘Physical layer security of space-division multiplexed fiber-optic communication systems in the presence of multiple eavesdroppers,’ in *2015 IEEE Global Communications Conference (GLOBECOM)*, San Diego, CA, USA: IEEE, Dec. 2015. DOI: 10.1109/GLOCOM.2015.7417679.
- [37] K. Guan, A. M. Tulino, P. J. Winzer and E. Soljanin, ‘Secrecy capacities in space-division multiplexed fiber optic communication systems,’ *IEEE Transactions on Information Forensics and Security*, vol. 10, no. 7, pp. 1325–1335, 2015.
- [38] J. Cho, K. Guan, S. Chandrasekhar and P. J. Winzer, ‘Experimental demonstration of physical-layer security in a fiber-optic link by information scrambling,’ in *ECOC 2016; 42nd European Conference on Optical Communication*, VDE, 2016, pp. 1–3.
- [39] S. Rothe, N. Koukourakis, H. Radner, A. Lonnstrom, E. Jorswieck and J. W. Czarske, ‘Physical layer security in multimode fiber optical networks,’ *Scientific Reports*, vol. 10, 2740, Feb. 2020. DOI: 10.1038/s41598-020-59625-9.
- [40] N. K. Fontaine, R. Ryf, H. Chen, D. T. Neilson, K. Kim and J. Carpenter, ‘Laguerre-Gaussian mode sorter,’ *Nature Communications*, vol. 10, 1865, Apr. 2019. DOI: 10.1038/s41467-019-09840-4.
- [41] J. Carpenter, B. J. Eggleton and J. Schröder, ‘110x110 optical mode transfer matrix inversion,’ *Optics Express*, vol. 22, no. 1, pp. 96–101, 2014. DOI: 10.1364/OE.22.000096.
- [42] T. A. Birks, I. Gris-Sánchez, S. Yerolatsitis, S. Leon-Saval and R. R. Thomson, ‘The photonic lantern,’ *Advances in Optics and Photonics*, vol. 7, no. 2, pp. 107–167, 2015.
- [43] E. Telatar, ‘Capacity of multi-antenna Gaussian channels,’ *European Transactions on Telecommunications*, vol. 10, no. 6, pp. 585–595, Nov. 1999. DOI: 10.1002/ett.4460100604.
- [44] C. Windpassinger, R. Fischer, T. Vencel and J. Huber, ‘Precoding in multiantenna and multiuser communications,’ *IEEE Transactions on Wireless Communications*, vol. 3, no. 4, pp. 1305–1316, Jul. 2004. DOI: 10.1109/TWC.2004.830852.

- [45] A. Abdelaziz and C. E. Koksál, ‘Fundamental limits of covert communication over MIMO AWGN channel,’ in *2017 IEEE Conference on Communications and Network Security (CNS)*, IEEE, Oct. 2017. DOI: 10.1109/cns.2017.8228657.
- [46] K.-P. Ho, J. M. Kahn, I. Kaminow, T. Li and A. Willner, ‘Mode coupling and its impact on spatially multiplexed systems,’ *Optical Fiber Telecommunications VI*, vol. 17, pp. 1386–1392, 2013.
- [47] D. Loterie, S. Farahi, I. Papadopoulos, A. Goy, D. Psaltis and C. Moser, ‘Digital confocal microscopy through a multimode fiber,’ *Optics Express*, vol. 23, no. 18, pp. 23 845–23 858, 2015.
- [48] J. W. Czarske, D. Haufe, N. Koukourakis and L. Büttner, ‘Transmission of independent signals through a multimode fiber using digital optical phase conjugation,’ *Optics Express*, vol. 24, no. 13, pp. 15 128–15 136, 2016.
- [49] Y. Zhou, B. Braverman, A. Fyffe, R. Zhang, J. Zhao, A. E. Willner, Z. Shi and R. W. Boyd, ‘High-fidelity spatial mode transmission through a 1-km-long multimode fiber via vectorial time reversal,’ *Nature Communications*, vol. 12, no. 1, pp. 1–7, 2021.
- [50] M. N’Gom, T. B. Norris, E. Michielssen and R. R. Nadakuditi, ‘Mode control in a multimode fiber through acquiring its transmission matrix from a reference-less optical system,’ *Optics Letters*, vol. 43, no. 3, pp. 419–422, 2018.
- [51] T. Čizmár and K. Dholakia, ‘Shaping the light transmission through a multimode optical fibre: Complex transformation analysis and applications in biophotonics,’ *Optics Express*, vol. 19, no. 20, pp. 18 871–18 884, 2011.
- [52] E. Jorswieck, A. Lonnstrom, K.-L. Besser, S. Rothe and J. W. Czarske, ‘Achievable physical-layer secrecy in multi-mode fiber channels using artificial noise,’ in *2021 17th International Symposium on Wireless Communication Systems (ISWCS)*, Berlin, Germany: IEEE, Sep. 2021. DOI: 10.1109/ISWCS49558.2021.9562176. arXiv: 2105.03137 [cs.IT].
- [53] H. Mahdaviifar and A. Vardy, ‘Achieving the secrecy capacity of wiretap channels using polar codes,’ *IEEE Transactions on Information Theory*, vol. 57, no. 10, pp. 6428–6443, Oct. 2011. DOI: 10.1109/TIT.2011.2162275. arXiv: 1007.3568 [cs.IT].
- [54] V. Bioglio, C. Condo and I. Land, ‘Design of polar codes in 5G new radio,’ *IEEE Communications Surveys & Tutorials*, vol. 23, no. 1, pp. 29–40, 2021. DOI: 10.1109/comst.2020.2967127. arXiv: 1804.04389 [cs.IT].
- [55] K.-L. Besser, S. Rothe, E. Jorswieck and J. W. Czarske. (2021). ‘Physical layer security on multi-mode fibers, Supplementary material,’ [Online]. Available: <https://github.com/k1b2/mmf-physec>.
- [56] R. Ryf, N. K. Fontaine, S. Wittek, K. Choutagunta, M. Mazur, H. Chen, J. C. Alvarado-Zacarias, R. Amezcua-Correa, M. Capuzzo, R. Kopf *et al.*, ‘High-spectral-efficiency mode-multiplexed transmission over graded-index multimode fiber,’ in *2018 European Conference on Optical Communication (ECOC)*, IEEE, 2018, pp. 1–3.
- [57] S. Sharifian, R. Safavi-Naini and F. Lin, ‘Post-quantum security using channel noise,’ in *Proceedings of the 2018 ACM SIGSAC Conference on Computer and Communications Security*, ser. CCS ’18, Toronto, Canada: Association for Computing Machinery, 2018, pp. 2288–2290. DOI: 10.1145/3243734.3278517.
- [58] D. E. B. Flaes, J. Stopka, S. Turtaev, J. F. De Boer, T. Tyc and T. Čizmár, ‘Robustness of light-transport processes to bending deformations in graded-index multimode waveguides,’ *Physical review letters*, vol. 120, no. 23, p. 233 901, 2018.
- [59] X.-T. Song, D. Wang, X.-M. Lu, D.-J. Huang, D. Jiang, L.-X. Li, X. Fang, Y.-B. Zhao and L.-J. Zhou, ‘Phase-coding quantum-key-distribution system based on Sagnac–Mach-Zehnder interferometers,’ *Physical Review A*, vol. 101, no. 3, 032319, Mar. 2020. DOI: 10.1103/PhysRevA.101.032319.
- [60] S. Rothe, H. Radner, N. Koukourakis and J. W. Czarske, ‘Transmission matrix measurement of multimode optical fibers by mode-selective excitation using one spatial light modulator,’ *Applied Sciences*, vol. 9, no. 1, 195, Jan. 2019. DOI: 10.3390/app9010195.
- [61] D. Gloge, ‘Weakly guiding fibers,’ *Applied optics*, vol. 10, no. 10, pp. 2252–2258, 1971.

- [62] S. Rothe, P. Daferner, S. Heide, D. Krause, F. Schmieder, N. Koukourakis and J. W. Czarske, ‘Benchmarking analysis of computer generated holograms for complex wavefront shaping using pixelated phase modulators,’ *Optics Express*, vol. 29, no. 23, pp. 37 602–37 616, 2021.
- [63] R. Brüning, D. Flamm, S. S. Ngcobo, A. Forbes and M. Duparré, ‘Rapid measurement of the fiber’s transmission matrix,’ in *Next-Generation Optical Communication: Components, Sub-Systems, and Systems IV*, SPIE, vol. 9389, 2015, pp. 110–116.
- [64] N. Koukourakis, T. Abdelwahab, M. Y. Li, H. Höpfner, Y. W. Lai, E. Darakis, C. Brenner, N. C. Gerhardt and M. R. Hofmann, ‘Photorefractive two-wave mixing for image amplification in digital holography,’ *Optics Express*, vol. 19, no. 22, pp. 22 004–22 023, 2011.
- [65] A. Thangaraj, S. Dihidar, A. Calderbank, S. McLaughlin and J.-M. Merolla, ‘Applications of LDPC codes to the wiretap channel,’ *IEEE Transactions on Information Theory*, vol. 53, no. 8, pp. 2933–2945, Aug. 2007. DOI: 10.1109/tit.2007.901143.
- [66] D. Klinc, J. Ha, S. W. McLaughlin, J. Barros and B.-J. Kwak, ‘LDPC codes for the Gaussian wiretap channel,’ *IEEE Transactions on Information Forensics and Security*, vol. 6, no. 3, pp. 532–540, Sep. 2011. DOI: 10.1109/tifs.2011.2134093.
- [67] F. Oggier, P. Sole and J.-C. Belfiore, ‘Lattice codes for the wiretap Gaussian channel: Construction and analysis,’ *IEEE Transactions on Information Theory*, vol. 62, no. 10, pp. 5690–5708, Oct. 2016. DOI: 10.1109/tit.2015.2494594.

## Supplementary Material

### 1 Characterisation of channel diagonalisation through SVD on varying fibre lengths

Diagonalisation of the TM allows Alice to transmit data to Bob specifically on certain spatial data streams. By multiplying the precoding matrix  $U^H$  to her desired message, Alice obtains the required mode combination, which she should launch with the SLM. Contrary to Eve, Bob does not have to perform channel inversion, but can decipher the received message by simply multiplying it with his decoding matrix  $V$ . This procedure compensates for modal crosstalk, the quality of which depends in particular on the diagonalisability. The question is: how well can Alice and Bob diagonalise their TM, i.e. their channel? For this investigation, MMFs of different lengths are chosen as data links between Alice and Bob, which are diagonalised by SVD-based pre- and decoding. An example of a diagonalised TM is shown in Fig. S1a. A high level of diagonalisability is achieved when a main diagonal entry of the TM corresponding to a data stream has a high value relative to its average background. For this purpose, the TM diagonalised by SVD is investigated row by row and the SNR for the respective data stream is calculated:

$$\begin{aligned} \text{SNR} &= 10 \cdot \log_{10} \left( \frac{P_{\text{data}}}{P_{\text{background}}} \right) \text{ dB} \\ &= 10 \cdot \log_{10} \left( \frac{\rho_{\text{data}}^2}{\mu_{\text{background}}^2} \right) \text{ dB}. \end{aligned} \quad (1)$$

The SNR is defined as relation between the power of the data stream  $P_{\text{stream}}$  and the background power  $P_{\text{background}}$ . The power in the data stream is determined by the square of the main diagonal element  $\rho_{\text{data}}$  according to the TM. The power in the background is determined by the average of the squared background elements  $\mu_{\text{background}}$ . The results are shown in Fig. S1b. They are based on 5 consecutive measurements for different MMF lengths (1 m, 10 m, 100 m).

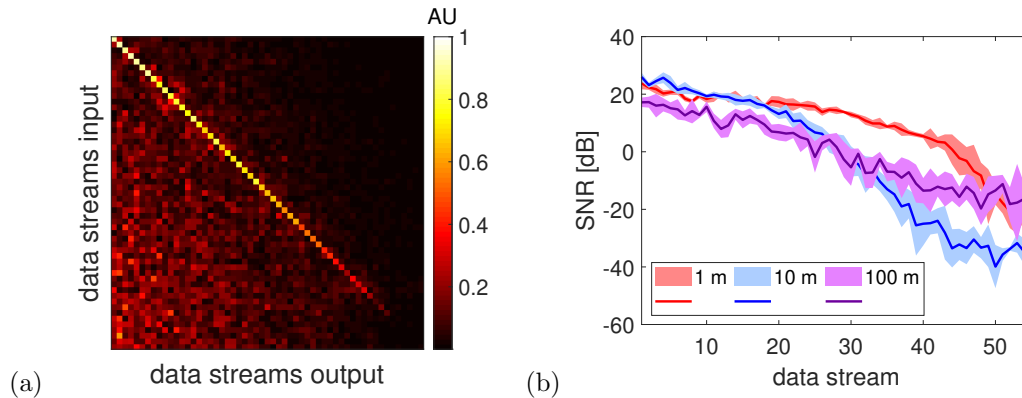


Figure S1: Investigation on SVD-based channel diagonalisation in dependence of varying MMF lengths. The diagonalisation is performed as shown in Fig. 1. (a) Measured TM between Alice and Bob at 1 m MMF after diagonalisation. (b) Evaluation of the SNR over available data streams. Mean values are indicated by the respective curve, whereas the standard deviation is given by the filled area around the curve. For each MMF length, 5 measurements were performed.

It can be shown that for all fibre lengths investigated, SVD-based diagonalisation can generate data streams with high SNR of up to 26 dB. However, due to MDL, a different number of available data streams with high SNR can be identified. While 44 data streams with positive SNR are available at 1 m MMF, there are only 24 at 100 m. We attribute this to the step-index profile of the MMFs under test. Step-index fibres are known to provide less stable light transport and are more susceptible to external influences such as temperature and mechanical stress compared to GRIN. With GRIN, the refractive



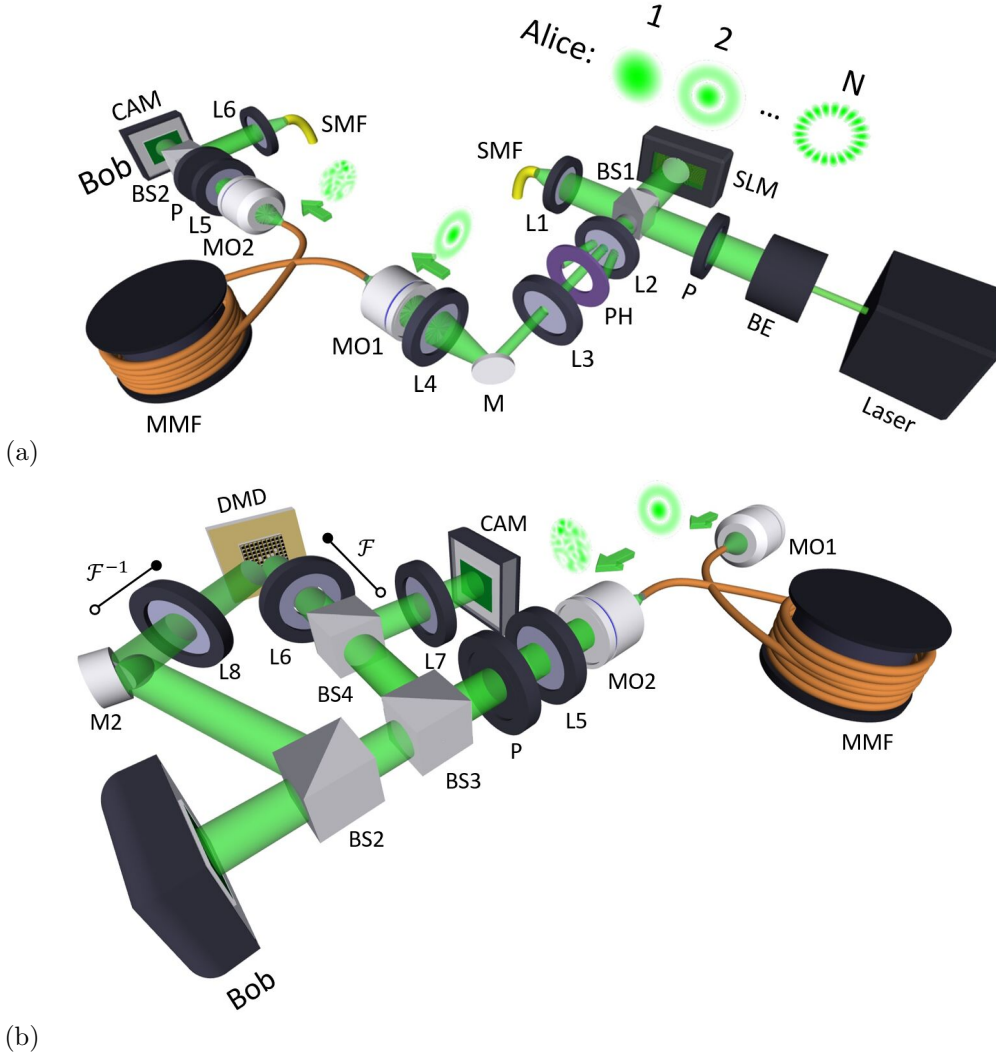


Figure S2: (a) Conventional scheme of the optical setup used for TM measurement. This setup was used for experiments on up to 10 m MMF. For measurements including Eve and a tapped MMF, the receiver-side was simply copied for Eve’s access. BE: beam expansion; P: linear polarisation filter; BS: beam splitter cube; L: lens; PH: pinhole; M: mirror; MO: microscope objective; CAM: CMOS camera (b) Common-path extension on the receiver-side for MMFs with increased length. As temporal fluctuations increase significantly in their frequency with longer fiber links, stability of the measurement scheme becomes an issue. Here, we propose a common-path solution applied to Bob’s side with which we have performed diagonalization experiments with 100 m MMF. DMD: digital micromirror device.

index profile is optimised for the transmission of multiple transverse modes. Thus, we expect that more data streams are suitable for data transmission at long GRIN MMFs.

## 2 Optical Setup

In Fig. S2a, the measurement scheme we used for our experiments is shown. A laser beam (LaserQuantum, Torus, 532 nm) is expanded that it exceeds the SLM (Holoeye, PLUTO) display and a plane illumination can be assumed. We use only one linear polarisation state, which means that we use only 50% of the available power. However, the system can easily be extended to consider the orthogonal state, as well [1],

[2]. Before the SLM is illuminated, the beam is split into object and reference by BS1. The reference is coupled into an SMF via lens L1. The length of the SMF is adjusted so that it interferes with the object beam and sufficient fringe contrast is ensured. Superpixel phase masks are displayed on the SLM for complex light field generation. Additionally, the masks are superimposed with a diffraction grating, since SLM pixels cause undesired diffraction orders, the polarisation filtering has a fidelity  $< 1$ , and the SLM has a fill factor  $< 1$ . This precaution allows the modulated light to be cleaned of the DC component. After propagation through L2, the  $+1^{\text{st}}$  diffraction order is spatially separated from DC and can be filtered with pinhole PH. The diameter is chosen that the superpixels merge into each other. After back transformation with L3, the light beam is imaged onto the MMF facet via a telescope system consisting of L4 and microscope objective (Mitutoyo 80x). The coupling angle is adjusted by mirror M. The coupling angle is ensured via an additional system that was presented in preliminary work [3], where the alignment procedure of the system is also explained.

On the receiver side (Bob), the emerging light field is imaged by a 4f configuration consisting of MO2 (Olympus 40x) and L5 onto a CMOS camera (IDS UI-3130). The polarisation state of the received light field is filtered according to the state on Alice's side. BS2 reunites object and reference beam in an off-axis configuration. This system was used to measure TMs of up to 10 m length. We considered phase drifting effects between object and reference beam as described in the main part. For measuring the TMs of the channels of both Alice/Bob and Alice/Eve, we simply copied the receiver setup for Eve and plugged the tapped MMF piece to it.

However, when the length of an MMF is increased to, for example 100 m, phase drifts increase in frequency, significantly. The reason for this is that fluctuations of the optical path of both fibres (MMF and SMF) are increased which lead to a high-frequency phase drift. The same phenomenon was observed by Borhani *et al.* [4] at 1 km MMF. Using the components from the aforementioned optical setup, the drift cannot be measured properly anymore due to limited response times. Therefore, we built a common-path system in which longitudinal optical path length fluctuations between object and reference are significantly reduced [5]. Unlike in conventional phase microscopes, the sample beam of an MMF does not always contain a composition of signal and DC components, which is why Fourier phase microscopes [6] or diffraction phase microscopes [5] cannot be applied as a common-path interferometer with an MMF. For measuring the TM of an MMF with common-path configuration, we have built an adaptive spatial filtering using a DMD. The emerging light field of an MMF is first split into object and reference by BS3. The reference part needs to be spatially filtered to achieve a Gaussian shape removing the speckled distribution. This is done by imaging the spatial frequency spectrum onto the surface of a DMD through L6 performing a Fourier transform (denoted with  $\mathcal{F}$  in Fig. S2b) The spectrum is observed by a telescope consisting of L6, L7 and a CMOS camera. For each sequence of TM measurement, the region in the spectrum with the highest intensity is selected and filtered by switching the respective DMD pixel to '1'. This procedure was inspired by the work from Nelsen *et al.* [7]. Afterwards, the reference beam is back-transformed through L8 ( $\mathcal{F}^{-1}$ ) and superimposed with the object beam on the camera generating a digital off-axis hologram.

### 3 Physical Layer Security

The model for our considered system is based on the MIMO wiretap channel model from wireless communications [8]. An illustration of the model can be found in Fig. S3.

Alice wants to transmit the codeword  $\mathbf{M} \in \mathbb{C}^n$  to the legitimate receiver Bob. She precodes the (modulated) codeword using matrix  $F_A \in \mathbb{C}^{n \times n}$  into signal  $\mathbf{X} = F_A \mathbf{M}$  that is then transmitted via the MMF. The received signals at Bob and eavesdropper Eve are given by

$$\mathbf{Y} = \tilde{H} \mathbf{M} + \mathbf{W}_b \quad (2)$$

$$\mathbf{Z} = \tilde{G} \mathbf{M} + \mathbf{W}_e, \quad (3)$$

respectively, where we use the shorthands  $\tilde{H} = \text{TM}_{AB} F_A$  and  $\tilde{G} = \text{TM}_{AE} F_A$ . The transmission channels from Alice to Bob and Eve are represented by the matrices  $\text{TM}_{AB}, \text{TM}_{AE} \in \mathbb{C}^{n \times n}$ , respectively. In our case, this corresponds to the MMF channels, where  $n$  is the number of supported modes. The terms  $\mathbf{W}_b, \mathbf{W}_e \in \mathbb{C}^n$  are independent circularly symmetric complex additive white Gaussian noise (AWGN) terms with identity covariance matrix.

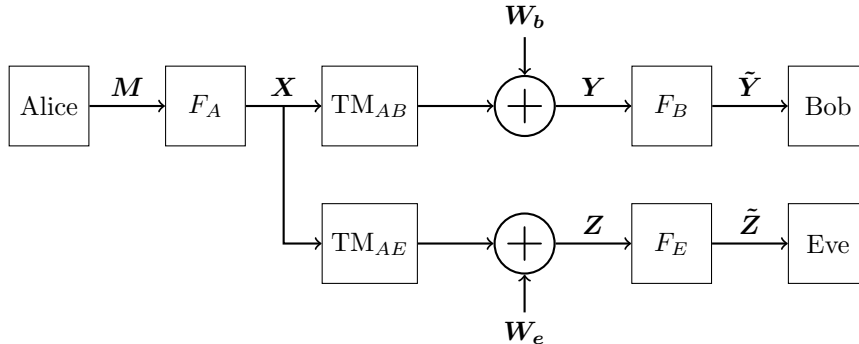


Figure S3: Considered wiretap channel model with a passive eavesdropper.

Next, Bob and Eve use the matrices  $F_B$  and  $F_E$ , respectively, to process their received signals. This way, they obtain the signals  $\tilde{\mathbf{Y}} = F_B \mathbf{Y}$  and  $\tilde{\mathbf{Z}} = F_E \mathbf{Z}$ , respectively.

The commonly used metric to analyze such channels is the *secrecy capacity*, which describes the fundamental limit of a secure communications such that Bob can reliably receive the data while simultaneously achieving an information-theoretic security against the eavesdropper [9, Chap. 3]. The secrecy capacity  $C_S$  for this system is given by [9, Cor. 3.1]

$$C_S = \max_{p_{\mathbf{X}}} \mathbb{I}(\mathbf{X}; \mathbf{Y} | \mathbf{Z}) = \max_{p_{\mathbf{X}}} (\mathbb{I}(\mathbf{X}; \mathbf{Y}) - \mathbb{I}(\mathbf{X}; \mathbf{Z})), \quad (4)$$

where  $\mathbb{I}(\mathbf{X}; \mathbf{Y})$  represents the mutual information between  $\mathbf{X}$  and  $\mathbf{Y}$  [10].

The solution to the above problem can be found explicitly when there is an average power constraint on the input signal. In literature the common assumptions are an average power constraint over all modes, i.e.,  $\sum_{i=1}^n \mathbb{E} [|x_i|^2] \leq nP$  [11], or a per-mode average power constraint, i.e.,  $\mathbb{E} [|x_i|^2] \leq P$  for all  $i$  [12]. However, in this work, we propose to use a different power constraint for the optical MMF system. Instead of an average power constraint, we suggest using a maximum power constraint in the form [13]

$$\sum_{i=1}^n |x_i(t)|^2 \leq P, \quad (5)$$

at all times  $t$ . The motivation behind this stems from the optical setup where a laser is employed at the transmitter and a camera at the receiver. First, the laser has a finite power output, and second, the camera is calibrated for a certain maximum power to avoid nonlinear fiber effects [14]. We, therefore, get the constraint that the total emitted laser power in each time slot may not be greater than a certain power  $P$ , which is described in (5).

While such a peak amplitude constraint has been considered in literature before, the solution to (4), i.e., the expression of the secrecy capacity, remains an open problem for this power constraint. For the standard AWGN point-to-point channel, some characterizations of the capacity are available [15]–[17]. For the non-fading wiretap channel, there also exist initial results on the secrecy capacity achieving input distributions [18]–[20]. In particular, it is shown in [18] that the optimal input distribution has a finite support. However, the optimal input distribution is unknown for the fading wiretap channel, which we consider in this work. Therefore, we resort to a well-known BPSK transmission scheme with finite support and investigate achievable secrecy rates  $R_S$  in the following section. In particular, we show that it is possible to securely transmit data at a positive rate over wiretapped MMF channels.

## 4 Secrecy Analysis – BPSK Transmission Scheme

In the following, we will provide an analysis of an achievable secrecy rate  $R_S$  over wiretapped MMFs. As described in Section 3, we consider a simple transmission scheme where Alice transmits BPSK symbols with SVD precoding. Since the precoding is designed for the channel to the legitimate receiver, Bob

chooses  $F_B$  accordingly. On the other hand, there is a mismatch to Eve. In order to compensate this, she applies a channel inversion to the received signal, i.e.,  $F_E = \tilde{G}^{-1}$ . By this strategy, she also diagonalises the channel with the side effect of noise amplification.

Since the resulting effective channels for both receivers are diagonal matrices, they can treat the data streams separately. For the aforementioned BPSK symbols, we can model the individual channels as binary symmetric channels (BSCs) with different bit-flip probabilities.

## 4.1 Transmitter Model

As discussed in Section 2.1, we implement an optical precoding matrix  $F_A$  as the right-singular vectors  $V$  of the channel  $\text{TM}_{AB}$  to Bob. Combined with the corresponding reception matrix  $F_B$  at Bob, the MMF channel is effectively diagonalised and separated into  $n$  parallel data streams. Alice now transmits BPSK symbols on  $K$  out of the  $n$  parallel streams. Let  $\mathcal{K} \subseteq \{1, \dots, n\}$  be an index set with  $|\mathcal{K}| = K$ . The indices in  $\mathcal{K}$  correspond to streams that we use for data transmission.

We now consider the BPSK example which fulfills the proposed power constraint (5) from Section 3 of having a maximum power  $P$  in each time slot. Specifically, we assume that the messages  $\mathbf{M}$  are BPSK symbols with

$$m_i(t) \in \{-p_i, +p_i\}, \quad \forall i \in \mathcal{K},$$

which yields

$$\sum_{i \in \mathcal{K}} |m_i(t)|^2 = P. \quad (6)$$

In order to transmit data, Alice selects the BPSK symbols on the individual modes (data streams) and adjusts the power of the laser accordingly. The SLM then optically applies the precoding. The resulting signal is transmitted via the MMF to Bob and Eve.

Since we do not assume knowledge of the eavesdropper's TM, Alice selects the power levels based on the singular values of the channel to Bob. Specifically, this is done by solving the optimization problem

$$\begin{aligned} \max \quad & \sum_{i=1}^K C_i \\ \text{s.t.} \quad & \sum_{i=1}^K p_i = P, \end{aligned} \quad (7)$$

where  $C_i$  are the channel capacities for the individual data streams. For our considered BPSK example, these capacities will be derived in the following.

## 4.2 Receiver Model

Since we used the right-singular vectors  $V$  of the channel to Bob as precoding at Alice, we need to multiply with the left-singular vectors  $U$  at Bob, i.e.,  $F_B = U^H$ . This way, we can diagonalise the legitimate channel and separate the data streams. On the other hand, Eve's channel cannot be diagonalised this way since there is a mismatch. Thus, the eavesdropper applies a channel inversion instead, i.e.,  $F_E = \tilde{G}^{-1}$ . With this, we get the received signals at Bob and Eve

$$\tilde{\mathbf{Y}} = F_B \mathbf{Y} = \Sigma \mathbf{M} + U^H \mathbf{W}_b \quad (8)$$

$$\tilde{\mathbf{Z}} = \tilde{G}^{-1} \mathbf{Z} = \mathbf{M} + \tilde{G}^{-1} \mathbf{W}_e, \quad (9)$$

respectively.

Since  $\Sigma$  is a diagonal matrix with the singular values  $\sigma_i$  on the main diagonal, we effectively diagonalised the channel to Bob. Recall that the matrix  $U$  with the left-singular vectors is a unitary matrix. The circular-symmetric Gaussian noise  $\mathbf{W}_b$  therefore keeps its properties under the transformation. On the other hand, the eavesdropper will experience a noise amplification due to the channel inversion  $\tilde{G}^{-1}$ .

### 4.3 Secrecy Rate

In the following, we will analyze the secrecy rate of the communication system described above. Since we are using BPSK, we transform the individual mode transmissions into BSCs. The data signals  $m_i$  are real and we are therefore only interested in the real part of  $\hat{m}_i$ . The probability of deciding for the wrong value of  $m_i$  at Bob is

$$\varepsilon_{B,i} = \Pr(\operatorname{Re}(\tilde{y}_i) > 0 \mid m_i = -p_i) \quad (10)$$

$$= \Pr(\operatorname{Re}(\tilde{w}_{b,i}) > \sigma_i p_i) \quad (11)$$

$$= Q\left(\frac{\sigma_i p_i}{\sqrt{\frac{1}{2} \operatorname{Re}(\Gamma)_{ii}}}\right) \quad (12)$$

$$= Q(\sigma_i p_i), \quad (13)$$

where the simplifications stem from the facts that  $\mathbf{W}_b$  is circularly symmetric and so is  $\tilde{W}_b = U^H \mathbf{W}_b$ ; additionally, we assume that  $\mathbf{W}_b$  has unit variance in both real and imaginary part, i.e., its covariance matrix is  $\Gamma = \mathbb{E}[\mathbf{W}_b \mathbf{W}_b^H] = 2I$ . Since  $U$  is a unitary matrix, the covariance matrix of  $\tilde{W}_b$  is the same.

The probability of deciding for the wrong value, based on the estimation  $\hat{m}_{e,i}$  at Eve is

$$\varepsilon_{E,i} = \Pr(\operatorname{Re}(\hat{m}_{e,i}) \neq m_i) \quad (14)$$

$$= \Pr(\operatorname{Re}(\tilde{w}_{e,i}) > p_i) \quad (15)$$

$$= Q\left(\frac{p_i}{\sqrt{\operatorname{Re}\left(\left(\tilde{G}^H \tilde{G}\right)^{-1}\right)_{ii}}}\right), \quad (16)$$

where we use  $\tilde{G}^{-1} \mathbf{W}_e \sim \mathcal{CN}\left(0, \left(\tilde{G}^H \tilde{G}\right)^{-1}\right)$ .

The capacity of a BSC with bit-flip probability  $\varepsilon_i$  is given by [10, Sec. 7.1.4]

$$C_i = 1 - H_b(\varepsilon_i), \quad (17)$$

where  $H_b$  is the binary entropy function. The secrecy rate  $R_S$  of mode  $i$  is then given by the difference of the channel capacities of Bob and Eve,

$$R_{S,i} = [C_{\text{Bob},i} - C_{\text{Eve},i}]^+ = [H_b(\varepsilon_{E,i}) - H_b(\varepsilon_{B,i})]^+. \quad (18)$$

Finally, the overall secrecy rate is the sum of the individual secrecy rates

$$R_S = \sum_{i \in \mathcal{K}} R_{S,i}. \quad (19)$$

## References

- [1] T. Čížmár and K. Dholakia, ‘Shaping the light transmission through a multimode optical fibre: Complex transformation analysis and applications in biophotonics,’ *Optics Express*, vol. 19, no. 20, pp. 18 871–18 884, 2011.
- [2] J. Carpenter, B. J. Eggleton and J. Schröder, ‘110x110 optical mode transfer matrix inversion,’ *Optics Express*, vol. 22, no. 1, pp. 96–101, 2014. DOI: 10.1364/OE.22.000096.
- [3] S. Rothe, H. Radner, N. Koukourakis and J. W. Czarske, ‘Transmission matrix measurement of multimode optical fibers by mode-selective excitation using one spatial light modulator,’ *Applied Sciences*, vol. 9, no. 1, 195, Jan. 2019. DOI: 10.3390/app9010195.

- [4] N. Borhani, E. Kakkava, C. Moser and D. Psaltis, ‘Learning to see through multimode fibers,’ *Optica*, vol. 5, no. 8, pp. 960–966, 2018.
- [5] G. Popescu, T. Ikeda, R. R. Dasari and M. S. Feld, ‘Diffraction phase microscopy for quantifying cell structure and dynamics,’ *Optics letters*, vol. 31, no. 6, pp. 775–777, 2006.
- [6] G. Popescu, L. P. Deflores, J. C. Vaughan, K. Badizadegan, H. Iwai, R. R. Dasari and M. S. Feld, ‘Fourier phase microscopy for investigation of biological structures and dynamics,’ *Optics letters*, vol. 29, no. 21, pp. 2503–2505, 2004.
- [7] B. Nelsen, A. Kabardiadi-Virkovski, T. Baselt, C. Taudt and P. Hartmann, ‘Kilohertz dynamic fourier filter for synthetic-aperture binary hologram reconstruction,’ in *Practical Holography XXXIII: Displays, Materials, and Applications*, International Society for Optics and Photonics, vol. 10944, 2019, 109440U.
- [8] F. Oggier and B. Hassibi, ‘The secrecy capacity of the MIMO wiretap channel,’ *IEEE Transactions on Information Theory*, vol. 57, no. 8, pp. 4961–4972, Aug. 2011. DOI: 10.1109/TIT.2011.2158487.
- [9] M. Bloch and J. Barros, *Physical-Layer Security*. Cambridge University Press, 2011. DOI: 10.1017/CB09780511977985.
- [10] T. M. Cover and J. A. Thomas, *Elements of Information Theory*, 2nd ed. Hoboken, NJ, USA: John Wiley & Sons, Inc., 2006. DOI: 10.1002/047174882X.
- [11] K. Guan, J. Cho and P. J. Winzer, ‘Physical layer security in fiber-optic MIMO-SDM systems: An overview,’ *Optics Communications*, vol. 408, no. June, pp. 31–41, Feb. 2018. DOI: 10.1016/j.optcom.2017.07.078.
- [12] K. Guan, P. J. Winzer, A. M. Tulino and E. Soljanin, ‘Physical layer security of space-division multiplexed fiber-optic communication systems in the presence of multiple eavesdroppers,’ in *2015 IEEE Global Communications Conference (GLOBECOM)*, San Diego, CA, USA: IEEE, Dec. 2015. DOI: 10.1109/GLOCOM.2015.7417679.
- [13] L. Li, S. M. Moser, L. Wang and M. Wigger, ‘On the capacity of MIMO optical wireless channels,’ *IEEE Transactions on Information Theory*, vol. 66, no. 9, pp. 5660–5682, Sep. 2020. DOI: 10.1109/tit.2020.2979716.
- [14] G. P. Agrawal, *Nonlinear Fiber Optics*, 4th ed. Academic Press, 2006. DOI: 10.1016/b978-0-12-369516-1.x5000-6.
- [15] A. Dytso, M. Al, H. V. Poor and S. Shamai (Shitz), ‘On the capacity of the peak power constrained vector Gaussian channel: An estimation theoretic perspective,’ *IEEE Transactions on Information Theory*, vol. 65, no. 6, pp. 3907–3921, Jun. 2019. DOI: 10.1109/TIT.2018.2890208. arXiv: 1804.08524 [cs.IT].
- [16] A. Dytso, M. Goldenbaum, H. Poor and S. Shamai (Shitz), ‘Amplitude constrained MIMO channels: Properties of optimal input distributions and bounds on the capacity,’ *Entropy*, vol. 21, no. 2, 200, Feb. 2019. DOI: 10.3390/e21020200.
- [17] A. Favano, M. Ferrari, M. Magarini and L. Barletta, ‘The capacity of the amplitude-constrained vector Gaussian channel,’ in *2021 IEEE International Symposium on Information Theory (ISIT)*, IEEE, Jul. 2021, pp. 426–431. DOI: 10.1109/ISIT45174.2021.9518071. arXiv: 2101.08643 [cs.IT].
- [18] O. Ozel, E. Ekrem and S. Ulukus, ‘Gaussian wiretap channel with amplitude and variance constraints,’ *IEEE Transactions on Information Theory*, vol. 61, no. 10, pp. 5553–5563, Oct. 2015. DOI: 10.1109/TIT.2015.2459705.
- [19] L. Barletta and A. Dytso, ‘Scalar Gaussian wiretap channel: Properties of the support size of the secrecy-capacity-achieving distribution,’ in *2021 IEEE Information Theory Workshop (ITW)*, IEEE, Oct. 2021. arXiv: 2109.01566 [cs.IT].
- [20] A. Favano, L. Barletta and A. Dytso, *On the capacity achieving input of amplitude constrained vector Gaussian wiretap channel*, Feb. 2022. arXiv: 2202.00586 [cs.IT].